ELSEVIER

Image and Vision Computing 17 (1999) 795–803

image AND vision COMPUTING

Size invariant circle detection

T.J. Atherton*, D.J. Kerbyson

Department of Computer Science, University of Warwick, Coventry CV4 7AL, UK

Received 10 February 1997; received in revised form 26 March 1998; accepted 27 August 1998

Abstract

The Circle Hough Transform (CHT) has become a common method for circle detection in numerous image processing applications. Various modifications to the basic CHT operation have been suggested which include: the inclusion of edge orientation, simultaneous consideration of a range of circle radii, use of a complex accumulator array with the phase proportional to the log of radius, and the implementation of the CHT as filter operations. However, there has also been much work recently on the definition and use of invariance filters for object detection including circles. The contribution of the work presented here is to show that a specific combination of modifications to the CHT is formally equivalent to applying a scale invariant kernel operator. This work brings together these two themes in image processing which have herewith been quite separate. Performance results for applying various forms of CHT filters incorporating some or all of the available modifications, along with results from the invariance kernel, are included. These are in terms of an analysis of the peak width in the output detection array (with and without the presence of noise), and also an analysis of the peak position in terms of increasing noise levels. The results support the equivalence between the specific form of the CHT developed in this work and the invariance kernel.

Keywords: Circle Hough Transform; Scale invariance; Circle detection in noise

1. The Circle Hough Transform

1.1. Background

The Circle Hough Transform (CHT) [1], aims to find circular formations, of a given radius R, within an image. An example of the conventional CHT is shown in Fig. 1. A set of edge points, within the original image, is indicated by the black circle. Each edge point contributes a circle of radius R to an output accumulator space, shown by the grey circles. The output accumulator space has a peak where these contributed circles overlap at the centre of the original circle.

The CHT can be formulated as a convolution whose binary mask coefficients are set on the circle boundary and are zero elsewhere. This convolution can be applied to an edge magnitude image (after suitable edge detection).

For the CHT calculation, a separate circle filter can be used for each radius of circle to be detected. This forms the familiar 3-dimensional parameter space, usually associated with the CHT, where two dimensions represent the position of the circle centre (a_x, a_y), and the third its radius (R).

$$(x - a_x)^2 + (y - a_y)^2 = R^2 \tag{1}$$

1.2. Modifications to the Circle Hough Transform

Modifications to the CHT have been widely implemented [2–4]. Such modifications have been made to either increase the detection rate of the algorithm, or more commonly to reduce its computational complexity. Modifications have included:

- the use of edge orientation,
- the use of a single accumulator space for multiple radii,
- the use of phase to code for radii, and
- implementation as convolution operators (Hough transform filters).

1.2.1. The use of edge orientation

Use of edge orientation information was first suggested by Kimme et al. [7], who noted that the edge direction on the boundary of a circle points towards or away from the circle centre. This modification reduces computational requirements as only an arc need be plotted perpendicular to the edge orientation at a distance $\boldsymbol{R}$ from the edge point. In the

* Corresponding author.
E-mail address: tja@dcs.warwick.ac.uk (T.J. Atherton)

0262-8856/99/$ - see front matter
PII: S0262-8856(98)00160-7

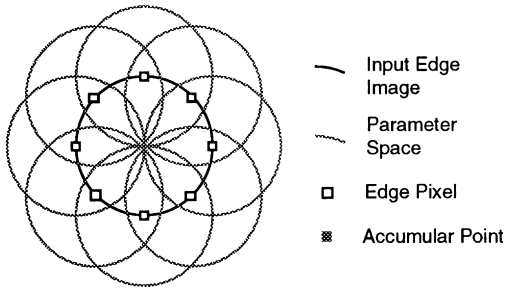

Fig. 1. The contribution of edge points to the accumulator space.

limit, arcs may be reduced to a single point in the accumulator space.

1.2.2. Use of a single accumulator space

Minor and Sklansky [5] extended the use of edge orientation and the limiting case of plotting a single point, by plotting a number of points on a line in the edge direction (a "spoke") to simultaneously detect circles over a range of sizes. This has the added advantage of using a two- rather than a three-dimensional parameter space. The operation can be further extended to the detection of circle-like shapes (compact convex objects, or blobs). Efficient computational implementations have been suggested and implemented on parallel image analysis systems [6].

1.2.3. Use of phase to code for size

Atherton and Kerbyson introduced a complex phase coding (from 0 to 2π) along the length of each spoke to give a complex accumulator space [8]. The phase coding represents the size of the circle along the length of the spoke. Constructive accumulation occurs in the accumulator space when spokes intersect with the same phase, i.e. contributions to a point in the accumulator array are only in-phase if that point is the centre of a circle. This technique has superior noise response characteristics, increasing the detection rate over the above two techniques [9].

1.2.4. Hough transform filters

The conventional CHT can be formulated as a convolution operator, or Hough transform filter [10], for the detection of a circle of a single size; the detection of a range of circle sizes (which can be considered similar to the spoke filter); and the detection of a range of circle sizes using a complex phase coding. Jahn [11] has used similar Hough transform filters for detecting craters in planetary images.

1.3. Contribution of this work

The contribution of the work presented here is to show that a specific combination of modifications to the CHT is formally equivalent to applying a scale invariant kernel operator. This work brings together these two themes in image processing which so far have been quite separate. The structure of this article is as follows. In section two, we define filters that implement the modifications to the CHT introduced above. In section three, we show how the modified CHTs, implemented as convolution filters, may be applied to detect circles. In section four, we briefly review scale invariant operators and show how they may be used to detect circles in an image, and in section five, the results of which are presented below:

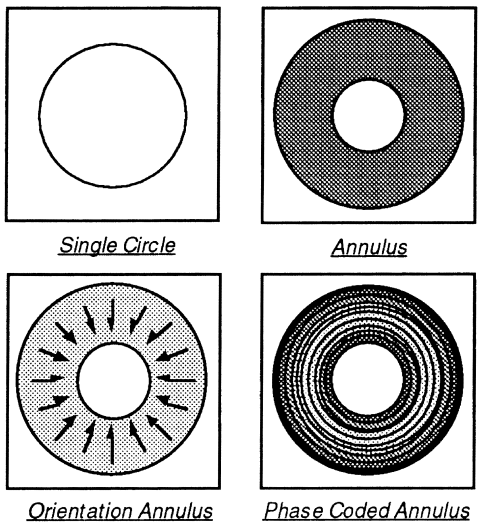

Fig. 2. Circle convolution operators.

- cross-sections of peak responses to a circle image without noise,
- typical test images and the response of the scale invariant filter,
- mean errors in detected position as noise levels increase,
- standard deviations of detected position as noise levels increase, and
- cross-sections of peak responses at a particular noise level.

Appendix A shows formally that a particular modified form of the CHT is equivalent to a circularly symmetric scale invariant filter (one of the Fourier-Mellin kernels).

2. Filters for circle detection

CHT techniques for the detection of a circle of single radius, the detection of a range of circle sizes, the use of orientation information, and the complex coding of size in terms of phase, can each be expressed in terms of a convolution operator or set thereof. Each of which are defined below.

It is assumed that the convolution operator size is $(2R_{max} + 1)$ by $(2R_{max} + 1)$, where R_{max} is the radius of the largest circle being considered, and that the centre of the operator is indexed (0,0). The convolution operators considered are:

- Single Circle (O_{sc}),
- Annulus (O_A),

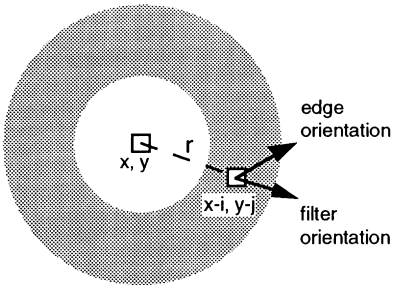

Fig. 3. Contribution of a single edge point to the convolution operation.

- vector Orientation Annulus ($\boldsymbol{O}_{\mathrm{OA}}$), and
- complex Phase Coded Annulus (O_{PCA}).

The form of each of these filters is shown in Fig. 2. It should be noted that the vector orientation annulus consists of two components (indicated by the arrows), and that the complex phase coding requires a real and imaginary part (indicated by the intensity change across the width of the annulus).

We first describe each of the basic CHT filter kernels below. In the next section, we describe the use of these filter kernels both singly (single circle, annulus, and orientation annulus), and in combination with each other (the orientation annulus together with the phase coded annulus).

Single circle – Detection of circles of a single radius

$$O_{\mathrm{SC}}(m,n) = 1 \; \textit{iff} \; (R-0.5)^2 < m^2 + n^2 < (R+0.5)^2 \quad (2)$$

$$O_{\mathrm{SC}}(m,n) = 0 \text{ otherwise}$$

Annulus – Detection of circles within a range of radii.

$$O_{\mathrm{A}}(m,n) = 1 \; \textit{iff} \; R_{\min}^2 < m^2 + n^2 < R_{\max}^2; R_{\max} > R_{\min} + 1 \quad (3)$$

$$O_{\mathrm{A}}(m,n) = 0 \; \textit{otherwise}$$

where $R_{\min}$ and $R_{\max}$ define the minimum and maximum circle radius respectively.

Orientation annulus – Detects a range of radii of circles, as for the annulus, but also uses edge orientation information by taking the dot product between the edge orientation and an orientation field within the annulus. The convolution operator consists of a vector field containing two components, $\boldsymbol{O}_{\mathrm{OA}} = (O_{\mathrm{OA_X}}, O_{\mathrm{OA_Y}})^T$ of a unit vector at each position within the annulus. These are defined as:

$$O_{\mathrm{OA_X}}(m,n) = \cos\theta_{mn} \; \textit{iff} \; R_{\min}^2 < m^2 + n^2 < R_{\max}^2 \quad (4)$$

$$O_{\mathrm{OA_X}}(m,n) = 0 \text{ otherwise}$$

$$O_{\mathrm{OA_Y}}(m,n) = \sin\theta_{mn} \; \textit{iff} \; R_{\min}^2 < m^2 + n^2 < R_{\max}^2$$

$$O_{\mathrm{OA_Y}}(m,n) = 0 \text{ otherwise}$$

where $\theta_{mn} = \tan^{-1}(n/m)$

Phase coded annulus – Detects a range of radii of circles by using phase to code for radius. Using a phase coding results in a complex convolution operator having a real and imaginary part for each operator coefficient. The real and imaginary parts of the phase coded annulus are defined as:

$$O_{\mathrm{PCA}}(m,n) = \exp[\mathrm{i}\varphi_{mn}] \; \textit{iff} \; R_{\min}^2 < m^2 + n^2 < R_{\max}^2 \quad (5)$$

$$O_{\mathrm{PCA}}(m,n) = 0 \text{ otherwise}$$

Two techniques for coding phase across the annulus, a linear coding and a ramped ('chirp') coding, have previously been investigated [10]. For a linear phase coding, φ_{mn} is given by:

$$\varphi_{mn}^{\mathrm{linear}} = 2\pi\left(\frac{\sqrt{m^2+n^2} - R_{\min}}{R_{\max} - R_{\min}}\right) \quad (6)$$

the ramped phase coding φ_{mn} is given by:

$$\varphi_{mn}^{\mathrm{ramped}} = 2\pi\left(\frac{\sqrt{m^2+n^2} - R_{\min}}{R_{\max} - R_{\min}}\right) \times \left(\frac{R_{\min}}{R_{\max}} + \frac{\left(1 - \frac{R_{\min}}{R_{\max}}\right)\left(\sqrt{m^2+n^2} - R_{\min}\right)}{R_{\max} - R_{\min}}\right) \quad (7)$$

A log phase coding has interesting properties, and also has a formal basis in invariance theory, which is discussed in section four. A log phase coding, φ_{mn}, is given by:

$$\varphi_{mn}^{\mathrm{logr}} = 2\pi\left(\frac{\log\left[\sqrt{(m^2+n^2)}\right] - \log R_{\min}}{\log R_{\max} - \log R_{\min}}\right) \quad (8)$$

3. Applying the circle detection filters

The convolution operators introduced in the previous section are applied to either an edge magnitude image, $\|\mathbf{E}\|$, where $\mathbf{E} = (E_x, E_y)^T$, or the partial gradient image in x and y (E_x and E_y, respectively). No edge thresholding operation is required in this work.

The operators for a single circle, an annulus, and a phase coded annulus can each be convolved with the edge magnitude image to give the following results, i.e.

$$Q_{\mathrm{SC}} = \|\mathbf{E}\| \otimes \frac{1}{r} O_{\mathrm{SC}} \quad (9)$$

$$Q_{\mathrm{A}} = \|\mathbf{E}\| \otimes \frac{1}{r} O_{\mathrm{A}} \quad (10)$$

$$Q_{\mathrm{PCA}} = \|\mathbf{E}\| \otimes \frac{1}{r} O_{\mathrm{PCA}} \quad (11)$$

where Q_{SC}, Q_{A}, Q_{PCA} are the outputs from the three convolutions, respectively. The 1/r factor normalises for circle

circumference, thus producing a similar response for circles of different radii.

It should be noted however, that O_{PCA} is a complex convolution operator and results in a complex output. The phase of this output contains information about the size of the detected circle, whilst its magnitude can be treated in the same way as the output of any CHT accumulator array.

The operator for the orientation annulus requires the dot product between the image gradient and the (radial) vector orientation annulus. This can be more easily understood by considering Fig. 3. The total contribution made to a single accumulator point (x, y) is the sum of all individual contributions from each point in the original image:

$$Q_{\mathrm{OA}}(x,y) = \sum_i \sum_j \mathbf{E}^T(i,j) \frac{1}{r(x-i,y-j)} \mathbf{O}_{\mathrm{OA}}(x-i,y-j) \tag{12}$$

where $r(m,n) = (m^2 + n^2)^{0.5}$.

Expanding the dot product, Eq (12) can be written as the sum of two convolutions – the first between the gradient image in x and the x-component of the orientation annulus, and the second between the gradient image in y and the y-component of the orientation annulus:

$$Q_{\mathrm{OA}} = E_x \otimes \frac{1}{r} O_{\mathrm{OA_X}} + E_y \otimes \frac{1}{r} O_{\mathrm{OA_Y}} \tag{13}$$

The orientation annulus and the phase coded annulus operators can be combined to give a phase coded orientation annulus operator. This combination results in a circle detection operator that uses both edge orientation information, and size information. It is a complex vector convolution operator, and to the knowledge of the authors, was first used for Hough transform shape detection in [10].

Consider a single edge point (i, j), and its contribution to a single output point in the phase coded orientation annulus accumulator array, $Q_{\mathrm{PCOA}}(x,y)$:

$$\mathbf{q}_{\mathrm{PCOA}}(x,y;i,j) = \left[\mathbf{E}^T(i,j) \frac{1}{r(x-i,y-j)} \mathbf{O}_{\mathrm{OA}}(x-i,y-j) \right] \times O_{\mathrm{PCA}}(x-i,y-j) \tag{14}$$

This is the dot product between the edge image and the vector orientation annulus, but is now also multiplied (or coded) by the complex phase coded annulus. The summation of all points contributing to the single accumulator point is then:

$$Q_{\mathrm{PCOA}}(x,y) = \sum_i \sum_j \left[\mathbf{E}^T(i,j) \frac{1}{r(x-i,y-j)} \mathbf{O}_{\mathrm{OA}}(x-i,y-j) \right] \times O_{\mathrm{PCA}}(x-i,y-j) \tag{15}$$

This may be expressed as two complex convolutions:

$$Q_{\mathrm{PCOA}} = E_x \otimes \left[\frac{1}{r} O_{\mathrm{OA_X}} O_{\mathrm{PCA}} \right] + E_y \otimes \left[\frac{1}{r} O_{\mathrm{OA_Y}} O_{\mathrm{PCA}} \right] \tag{16}$$

where there is a point-wise multiplication between both the components of the orientation annulus, $O_{\mathrm{OA_X}}$ and $O_{\mathrm{OA_Y}}$, and the complex phase coded annulus O_{PCA}.

4. Circle detection using invariance kernels

In this section we show that the Hough transform filters, that we and others have been using are either equivalent to, or closely related to, kernels derived from considering invariant transformations of patterns [12]. Such transformations, or deformations, include scaling, rotation, and translation. For circle detection the deformations of interest are rotation and scaling. Patterns that are circularly symmetric are inherently invariant to rotation. A kernel invariant to rotation and scaling will give a response that will be a peak at the centre of the circle, the magnitude of this peak will be invariant to the size of the circle (the response will vary with circle luminance, and phase at the peak will give a measure of the circle size). For recent reviews of invariants in pattern recognition see [13, 14]. A thorough introduction to this area is given by Rubenstein et al. [15] who show that the invariance kernel for scaling in two dimensions can be derived from the scaling group:

$$x' = \tau x \tag{17}$$

$$y' = \tau y$$

where (x, y) is the original coordinate, (x', y') the transformed coordinate, and τ the scaling factor. The Lie derivative, or generator for this group, is:

$$L_s = x \frac{\partial}{\partial x} + y \frac{\partial}{\partial y} \tag{18}$$

Rubenstein et al. [15] show that the invariance kernel for scaling in 2D is then:

$$K_{rs}(k,l) = \frac{1}{r^2} \exp[\mathrm{i}(k\theta + l \ln r)] \tag{19}$$

This is a family of invariance kernels (the so-called Fourier–Mellin transform) which, as rotation and scaling operations commute in 2D, is also shared by rotation. We choose a circularly symmetric member of this family by setting $k = 0$, and we limit consideration in this work to the first radial component:

$$K_{rs}(0,1) = \frac{1}{r^2} \exp[\mathrm{i}(l \ln r)] \tag{20}$$

We are taking the "d.c." response in theta, and the first Fourier coefficient in log radius, the phase of which signals log size. A change in circle size is transformed by

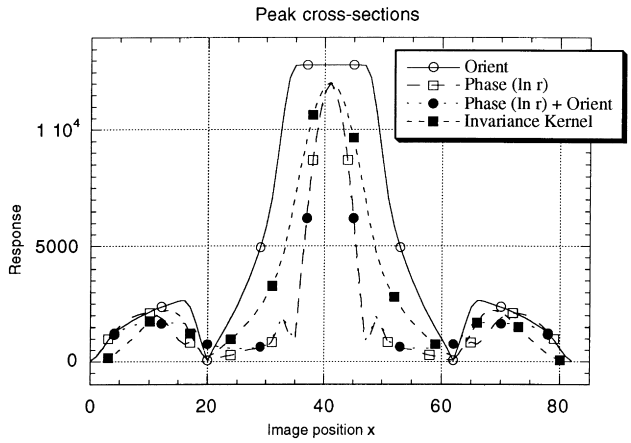

Fig. 4. Cross-sections of the peak in the convolution outputs.

this into a shift in log size, i.e. into a translation $r' = \tau r \rightarrow \log r' = \log r + \log \tau$. The kernel is shift variant (unlike for example the Fourier kernel) so it is applied to every point in the image in the form of a convolution. The resulting image has at each point, the convolution result $f(x,y) \otimes K_{rs}(0,1)$.

Motivated by the observation that the log of radius provides the phase of the invariance kernel we have examined the relationship between the Hough transform filters that utilise both edge orientation and log radial phase, and the invariance filter kernel for scaling. The two approaches are shown to be formally equivalent in Appendix A, subject to the constraints that phase in the Hough transform is proportional to log radius and considering the invariance kernel term $K_{rs}(0,1)$.

5. Comparative results

A number of experiments have been performed to investigate the behaviour of the techniques in terms of the width of the peak in the accumulator array, the height of the peak above the surrounding pedestal, and the accuracy of detecting the centre of the circle [16]. We report:

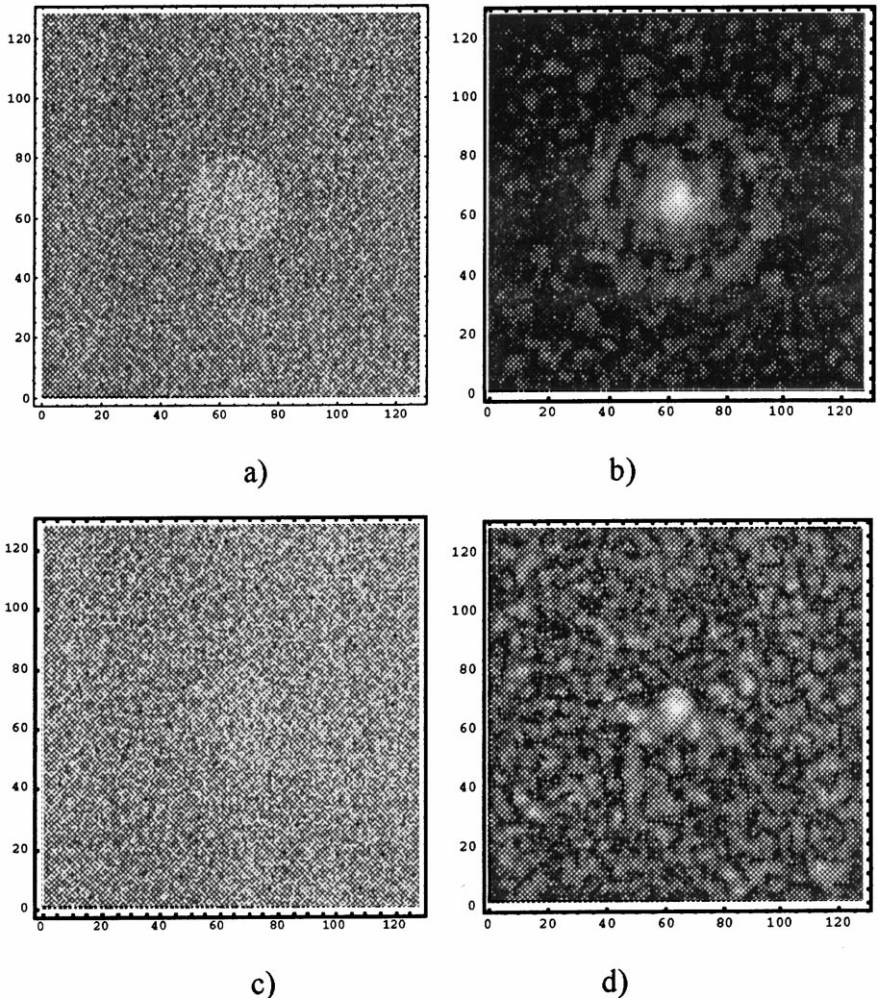

Fig. 5. a) Example circle image with added Gaussian noise variance of 3×10^4 and b) invariance kernel output c) Same circle image with added Gaussian noise variance of 3×10^5 and d) invariance kernel output.

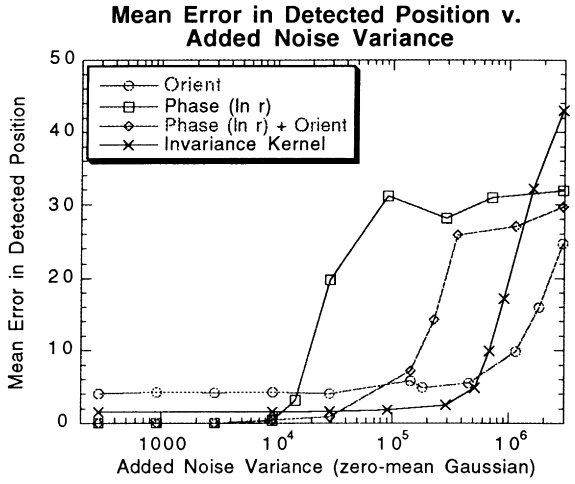

Fig. 6. Mean error in detected position relative to the true circle centre plotted against added noise variance.

1. Cross-sections of the responses of the convolution operations to ideal circle images (with no added noise).
2. Output arrays for noisy test images.
3. The positional accuracy of circle centre detection in the presence of additive noise.
4. The response peak widths and the surrounding "pedestal" of the background for a specific noise level.

The convolution operations used in the experiments were:

- orientation annulus,
- log radial phase coded annulus,
- log radial phase coded orientation annulus, and
- scale invariance kernel, $K_{rs}(0,1)$.

Results are presented from applying the convolution operations described above to an image of size 128 × 128 pixels, containing a circle of radius $R = 16$ pixels. The intensity of the background was set to zero, and the pixels within the circle were set to 255. The image was real to prevent underflow or overflow effects with the added noise. The operators were windowed in radius with a minimum $R_{\min}$, of 8 pixels, and a maximum, $R_{\max}$, of 24 pixels, the window was zero outside this range and unity between $R_{\min}$ and $R_{\max}$.

5.1. Peak response in the absence of noise

Each of the convolution operators were applied to an image containing a circle of radius 16 pixels but which contained no added noise. The cross-section of the resulting peak in the output for each of the convolutions is shown in Fig. 4.

The orientation annulus results in a peak width (full width at half-height) of 22 pixels which corresponds approximately to the width of the annulus of the operator ($R_{\max}$–$R_{\min}$). The phase coded annulus results in a narrower peak than that of the orientation annulus, 9 pixels (full width at half-height). This is due to the coherent integration (constructive and destructive integration) of the phase coding. Incorporating orientation into the phase coding has a relatively small effect on the width of the response peak. The invariance kernel generates a peak of slightly greater width, of 13 pixels (full width at half-height).

5.2. Detection of a circle in noise

The ideal circle image was used to analyse the effectiveness of the convolution operations to detect a circle in the presence of noise (Fig. 5). Zero-mean, white gaussian noise was added to vary the signal-to-noise ratio in the circle image. One possible measure of signal-to-noise ratio in this context can be found by taking the ratio of the energy response of the detection filter at the object centre due to a perfect noiseless circle centred on $\mathbf{x}_c$, $|y_s(\mathbf{x}_c)|^2$, and the mean square response of the filter-to-noise alone at this position, $E\{|y_n(\mathbf{x}_c)|^2\}$. The detection signal-to-noise ratio (SNR) is defined as [17]:

$$SNR = 10 \log\left(\frac{|y_s(\mathbf{x}_c)|^2}{E\{|y_n(\mathbf{x}_c)|^2\}} \right) \tag{21}$$

This SNR gives a measure of how the output signal peak stands out above the background noise pedestal, but suffers from the drawback that different detection techniques will produce different SNRs for a given added noise variance. This confounds the process of comparing, for example, the accuracy with which an object centre is detected as a function of SNR. We, therefore, report accuracy in positional detection as a function of added noise variance.

If for a circle centred on $\mathbf{x}_c$, the position of the peak response, in the detection filter output, is measured (on a particular trial) to be $\mathbf{x}_p$, we can gain further insight into the performance of the filters by estimating the mean radial error in the detected position over a number of trials:

$$\bar{r} = E\left\{ \left(\left(\mathbf{x}_p - \mathbf{x}_c \right)^2 \right)^{0.5} \right\} \tag{22}$$

A similar procedure can be used to estimate the variance σ_r^2 (or standard deviation, σ_r) of the mean error in detected position over a number of trials. If the distribution of the detected positions about the correct centre is approximately Gaussian (for any particular value of image noise), we would expect the mean error in detected position to be close to Rayleigh distributed. In this case the standard deviation of the mean error in position, σ_r, and the mean error in position, $\bar{r}$, will be approximately equal [18].

The amount of additive noise was varied over a range $\sigma_n^2 = 3.10^2$ to $\sigma_n^2 = 3.10^6$. The peak position in the output of each convolution operator was measured and the error between it and the expected circle centre was recorded. A Monte-Carlo style analysis was performed with 50 trials per experiment (500 trials per experiments for the invariance kernel), and the errors in detected position was recorded.

The mean error in detected position for each of the

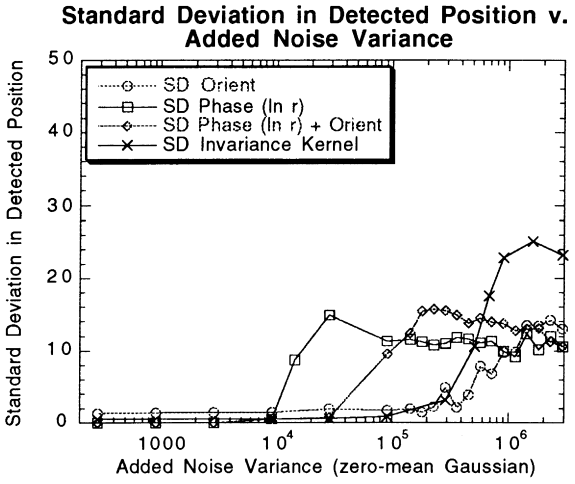

Fig. 7. Standard deviation in the detected positions relative to the true centre plotted against added noise variance.

techniques tested (Fig. 6), shows a region of accurate detection at low added noise variances (high SNR levels), with each method breaking down as the added noise variance is increased.

The standard deviation of the error in the detected position (Fig. 7), follows the same form as the mean error in the detected position (Fig. 6). Table 1 summarises the position detection errors for low added noise levels, and also shows the noise level at which the mean and standard deviation of the position error rise above 8 pixels. There is a qualitative similarity between the behaviour of the mean errors and their standard deviations (Figs. 6 and 7), and this is further borne out by the quantitative comparison of the noise levels at which the errors in positional detection rise above a threshold of 8 pixels (Table 1).

5.3. Peak widths in the presence of noise

The peak cross-sections in the presence of noise (Fig. 8), reveal the following about the peak widths and background levels for each of the techniques. The orientation annulus results in a broad peak which stands significantly above its background pedestal. The phase coded annulus is no longer a viable detector at these noise levels, revealed by the low peak height above the surrounding pedestal, which itself is significantly higher than the pedestal for the other techniques. The phase coded orientation annulus has a narrow peak width and low background level, as has the invariance kernel.

6. Discussion

We have reviewed a series of modifications to the CHT and shown that a combination of four of these, the inclusion of edge direction, simultaneously considering a range of radii, using a complex accumulator array with phase proportional to the log of radius, and implementation as a filter, is formally equivalent to applying a scale invariant kernel operator. The results presented provide qualitative support for this.

The inclusion of edge direction in a circle detector (sensitive to a range of radii), the “orientation annulus”, results in broad peaks but good noise tolerance. Introducing log radial phase to the CHT (also sensitive to a range of radii) results in narrower peak widths with a low noise tolerance. Combining these; edge direction, a range of radii, and log radial phase, results in narrow peak widths and significantly improved noise tolerance. We have shown that this version of the CHT is formally equivalent to an invariance kernel. The results show that the invariance kernel generates peaks in the accumulator array that are slightly broader than the combined CHT, but that it has superior noise performance. The differences between the two techniques are likely to be implementational, for example the Sobel operator was used to form estimates of image partial derivatives for the combined CHT, and it is known to be a poor edge orientation estimator [8,19].

The orientation annulus technique (a range of radii, and edge direction) would also be expected to benefit from the use of an improved edge estimator, however, it cannot provide estimates of circle size that are encoded in the phase at the peak location given by the phase techniques (an issue for further work).

We have investigated modifying the CHT to include edge direction, a range of radii, and log radial phase. We have shown that this technique is formally equivalent to a scale invariant filter kernel, and that this kernel gives a robust implementation of a circle detector at low signal-to-noise ratio. This equivalence between a form of the CHT and a rotation and scale invariant kernel, opens up the possibility for a more formal understanding of the detection of circular (and other) structures in images.

Table 1
Summary of mean positional errors for high SNR levels and noise levels at which the different techniques break down

	Mean position error (in pixels ±1 SE) when added noise variance = 9126	Mean position error exceeds 8 pixels at added noise variance	Standard deviation in position error exceeds 8 pixels at added noise variance
Orient	4 ± 1	8×10^5	6×10^5
Phase	1 ± 1	2×10^4	1×10^4
Phase + Orient	1 ± 1	1×10^5	8×10^4
Invariance kernel	1.5 ± 0.8	6×10^5	4×10^5

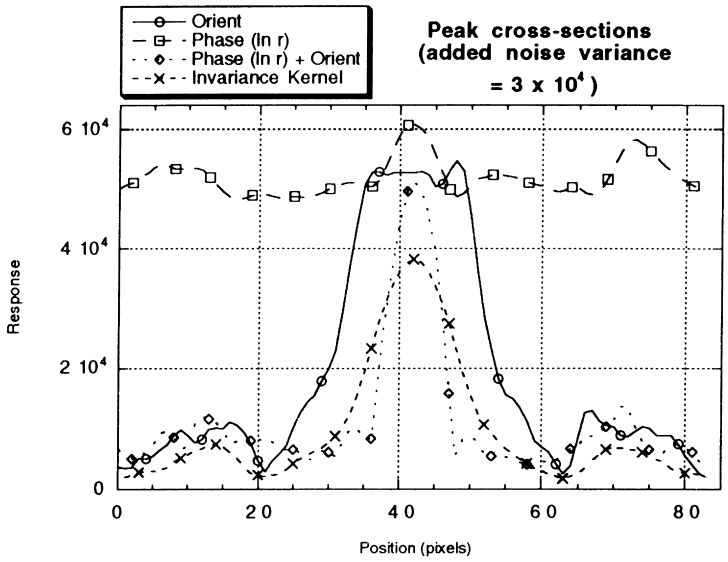

Fig. 8. Comparison of the peak cross-sections for added noise variance of 3×10^4.

Appendix A. Equivalence of Hough transform filters and invariance kernel

Under the specific conditions that we are using (Hough transform filter incorporating edge orientation and log radial phase, as described in the text) we show that the Hough transform filters are an exact implementation of the invariance kernel $K_{rs}(0,1)$.

The result of applying the orientation and log (r) phase Hough transform filters is:

$$Q_{\mathrm{PCOA}} = E_x \otimes \left[\frac{1}{r} O_{\mathrm{OA_x}} O_{\mathrm{PCA}} \right] + E_y \otimes \left[\frac{1}{r} O_{\mathrm{OA_Y}} O_{\mathrm{PCA}} \right] \tag{A.1}$$

which can be written as:

$$Q_{\mathrm{PCOA}} = \frac{\partial f(x,y)}{\partial x} \otimes \left[\frac{1}{r} \left(\frac{x}{r} \right) \exp[\mathrm{i} \ln r] \right] + \frac{\partial f(x,y)}{\partial y} \otimes \left[\frac{1}{r} \left(\frac{y}{r} \right) \exp[\mathrm{i} \ln r] \right] \tag{A.2}$$

or

$$Q_{\mathrm{PCOA}} = f(x,y) \otimes \left[\frac{\partial}{\partial x} \left(\frac{x}{r^2} \right) \exp[\mathrm{i} \ln r] \right] + f(x,y) \otimes \left[\frac{\partial}{\partial y} \left(\frac{y}{r^2} \right) \exp[\mathrm{i} \ln r] \right] \tag{A.3}$$

After some manipulation this is:

$$Q_{\mathrm{PCOA}} = f(x,y) \otimes \left[i \left(\frac{1}{\boldsymbol{r}^2} \right) \exp[\boldsymbol{i} \ln r] \right] = \mathrm{i} K_{rs}(0,1) \tag{A.4}$$

Eq (A.4) is the required result. The Hough transform filters, under the conditions we have given, are equivalent to the one of the invariance kernels for the image deformation of scaling.

References

[1] R.O. Duda, P.E. Hart, Use of the Hough Transform to Detect Lines and Curves in Pictures, Communications of the ACM 15 (1972) 11–15.
[2] E.R. Davies, A Modified Hough Scheme for General Circle Location, Pattern Recognition Letters 7 (1988) 37–43.
[3] P. Kierkegaard, A Method for Detection of Circular Arcs Based on the Hough Transform, Machine Vision Applications 5 (1992) 249–263.
[4] H.K. Yuen, et al., A comparative study of Hough transform methods for circle finding, in: Proc. Alvey Vision Conference, ALVEY, 1989, pp. 169–174.
[5] L.G. Minor, J. Sklansky, Detection and segmentation of blobs in infrared images, IEEE Trans. SMC 11 (1981) 194–201.
[6] T.J. Atherton, et al., Detection and segmentation of blobs using the Warwick Multiple-SIMD Architecture, in: Parallel Architectures for Image Processing, vol. 1246, SPIE, 1990, pp. 96–104.
[7] C. Kimme, D. Ballard, J. Sklansky, Finding circles by an array of accumulators, Proc. ACM 18 (1975) 120–122.
[8] T.J. Atherton, D.J. Kerbyson, Using phase to represent radius in the coherent circle Hough transform, in: Proc, IEE Colloquium on the Hough Transform, IEE, London, 1993.
[9] T.J. Atherton, D.J. Kerbyson, The coherent circle Hough transform, in: British Machine Vision Conference, BMVA Press, 1993.
[10] D.J. Kerbyson, T.J. Atherson, Circle detection using Hough transform filters, in: 5th Int. Conf. On Image Processing and its Applications, Edinburgh, 1995.
[11] H. Jahn, in: Proc. ISPRS Commission III Symposium on Spatial Information from Digital Photogrammetry and Computer Vision Crater Detection by Linear Filters Representing the Hough Transform, vol. 2357, SPIE, Munich, 1994, pp. 427–431.
[12] W.C. Hoffman, The Lie algebra of visual perception, J. Mathematical Psychology 3 (1966) 65–98.
[13] J. Wood, Invariant pattern recognition: a review, Pattern Recognition 29 (1) (1996) 1–17.
[14] D. Forsyth, J.I. Mundy, A. Zisserman, Transformational invariance—a primer, Image and Vision Computing 10 (1992) 39–45.
[15] J. Rubinstein, J. Segman, Y. Zeevi, Recognition of distorted patterns by invariance kernels, Pattern Recognition 24 (1991) 959–967.

[16] E.R. Davies, Modelling peak shapes obtained by Hough transform, IEE Proceeding-E 139 (1992) 9–12.
[17] C.W. Therrien, Discrete random signals and statistical signal processing, in: A.V. Oppenheim (Ed.), Prentice Hall Signal Processing Series, Prentice Hall, Englewood Cliffs, 1992.
[18] A. Papoulis, Probability, Random Variables and Stochastic Processes, McGraw-Hill, Polytechnic Institute of Brooklyn, 1965.
[19] J. Kittler, On the accuracy of the Sobel Edge Detector, Image and Vision Computing 1 (1983) 37–41.